CCS Chemistry

RESEARCH ARTICLE

Received: Mar. 2, 2022 | Accepted: Apr. 5, 2022 | Published: May 10, 2022

# Interfacial Reinitiation of Free Radicals Enables the Regeneration of Broken Polymeric Hydrogel Actuators

Baoyi Wu[1,2], Huanhuan Lu[1,2], Yukun Jian[1,2], Dachuan Zhang[1], Yu Peng[1,2], Jie Zhuo[1,2], Xiaoxia Le[1,2], Jiawei Zhang[1,2]*, Patrick Théato[3,4]* & Tao Chen[1,2]*

[1]*Key Laboratory of Marine Materials and Related Technologies, Zhejiang Key Laboratory of Marine Materials and Protective Technologies, Ningbo Institute of Materials Technology and Engineering, Chinese Academy of Sciences, Ningbo 315201,* [2]*School of Chemical Sciences, University of Chinese Academy of Sciences, Beijing 100049,* [3]*Soft Matter Synthesis Laboratory, Institute for Biological Interfaces III, Karlsruhe Institute of Technology (KIT), D-76344 Eggenstein-Leopoldshafen,* [4]*Institute for Chemical Technology and Polymer Chemistry, Karlsruhe Institute of Technology (KIT), D-76131 Karlsruhe*

**Corresponding authors: zjwmail163@163.com; patrick.theato@kit.edu; tao.chen@nimte.ac.cn*

**Cite this:** *CCS Chem.* **2023**, 5, 704–717
**DOI:** 10.31635/ccschem.022.202201942

**Living organisms, from plants to animals, have inspired and guided the design and fabrication of polymeric hydrogels with biomimetic morphology, shape deformation, and actuation behavior. However, the existing polymeric hydrogels are fragile and vulnerable, which seriously hinders further application. Therefore, endowing hydrogels with a biomimetic self-growth property and regenerating the macroscopic shape of hydrogels after they suffer significant damage are highly desirable for the next generation of adaptive biomimetic hydrogels. Inspired by the tail regeneration of geckos, we herein report an efficient and universal strategy of interfacial diffusion polymerization (IDP), which can regenerate the polymeric layer at a solid–liquid interface, thereby growing new hydrogels on the existing hydrogel layers. Through changing the solvent viscosity and/or monomer type of the hydrogel precursor, diverse new hydrogels have been regenerated to endow the initial hydrogels with additional fluorescent functions and/or actuating properties. Due to the high efficiency and universality of IDP, an injured hydrogel actuator can be repaired, regenerated, and recovered to its initial condition, even after suffering severe damage such as cutting or piercing. We believe that the regeneration strategy of polymeric hydrogels will inspire the design of biomimetic materials and motivate the fabrication of the next generation of soft robots with adaptive and multifunctional properties.**

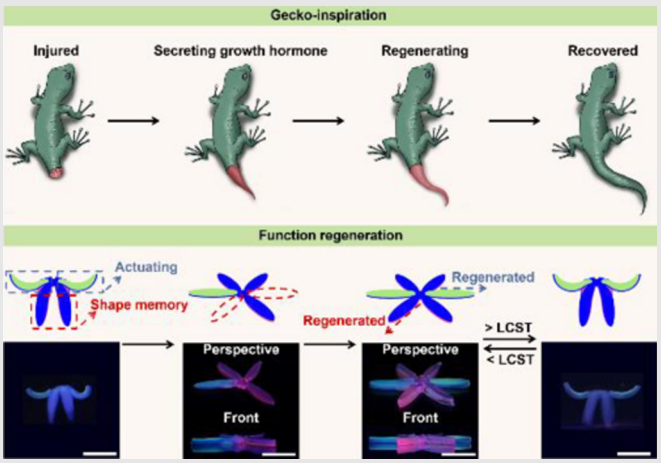


*Keywords:* hydrogels, biomimetics, interface, diffusion polymerization, free radicals monitor

## Introduction

Nature is an unlimited source of inspiration and has guided the design and fabrication of versatile intelligent artificial materials.[1-9] Hydrogel actuators,[10-12] which are one of the most promising classes of such bionic materials,[13,14] can imitate the morphology and deformation of biological organisms due to their wet and soft properties.[15-19] However, most of the existing hydrogel actuators are fragile and vulnerable, which seriously hinders the development of hydrogel actuators in complex situations.[20-27] As one of the most promising bionic materials, self-healing hydrogels can repair themselves when the damaged parts are close enough to form chemical bonds or noncovalent interactions but can not regenerate a missing part when the hydrogel suffers from huge damage. Besides, the existing self-healing hydrogels usually require that the damage be fresh; otherwise, the self-healing becomes more and more inefficient.[28-31] By contrast, although biological organisms also suffer from huge damage, the injured parts can still recover to their initial state via body metabolism. Moreover, biological organisms can also exhibit self-growth properties which are capable of endowing them with brand new functions.[32,33] For example, tadpoles only breathe through their gills and swim under water, propelling themselves with their tails. Interestingly, after metamorphosis, tadpoles grow into frogs, who breathe through their lungs and jump with their limbs. Inspired by this growth behavior of biological organisms, the development of next-generation bionic hydrogel actuators with self-growing properties is receiving immense scientific attention.[34-36]

In order to realize the self-growth and functionalization of the as-prepared hydrogels, the reinitiation of the polymerization and a tough interfacial interaction between original hydrogel and newly generated hydrogel are unavoidable.[37-46] Recently, a few strategies have been proposed successfully. For example, Gong and coworkers regenerated mechano-radicals and reinitiated polymerization by force-induced polymer strand scission.[37] A double-network hydrogel containing monomer was subjected to repetitive mechanical loading that destroyed the polymer chains and induced the generation of mechano-radicals, which reinitiated the polymerization of the monomer. Further, Daraio and coworkers utilized the photosynthesis of embedded chloroplasts to reproduce glucose inside a hydrogel network and remodel microstructures under white light exposure.[38] Also, Zarket and Raghavan proposed an inside-out technique for creating multilayered polymer capsules.[39] Although the above-mentioned studies proposed the possibility of linking/reconstructing the hydrogel layers with firm interfacial toughness, the polymerization mechanism and applications were still unclarified, which limited the further development of self-growth hydrogel. Therefore, to propose an efficient and universal techniques for the growth of the macroscopic shape of as-prepared hydrogels remains a challenge.

Inspired by the tail regeneration of the gecko that can secrete and transport growth hormone to its injured part and regenerate a new tail by the division of cells in the injured part (Scheme 1a), herein, an efficient strategy is proposed that endows hydrogels with such a self-growing property via an interfacial diffusion polymerization (IDP). Different from other reported methods that reinitiate the polymerization within the hydrogel, free radicals in the IDP strategy were generated via a redox reaction at the solid–liquid interface between ammonium persulphate (APS) in an as-prepared hydrogel and *N*,*N*,*N*′,*N*′-tetramethylethylenediamine (TEMED) in another hydrogel precursor (Scheme 1b). Here, the initiating polymerization at the solid–liquid interface exhibits several advantages. (1) The new hydrogel could grow on the surface of the initial hydrogel and increase the macroscopic volume of the whole system. (2) The hydrogel precursor could fully moisten the initial hydrogel surface and prevent oxygen from getting in, which commonly acts as a polymerization inhibitor. (3) Polymerization at the solid–liquid interface could enhance the interfacial interaction between two layers, thereby generating a unique interpenetrating network at the interface. (4) This approach represents a universal strategy that can be adapted to generate diverse new hydrogels on hydrogel-based substrates and hydrophilic substrates. (5) Such an IDP strategy could custom repair an injured hydrogel actuator. Different from those self-healing hydrogels that require fresh damage and potential self-healing factors such as supramolecular interaction or dynamic covalent bonds,[47,48] any injured hydrogel actuators could be repaired and recover to their initial condition both in macroscopic shape and chemical structure and continue functioning via IDP. We believe this will provide a new vision and inspire the fabrication of the next generation of adaptive robots, multifunctional hydrogel actuators, and biomimetic systems.

## Experimental Methods

### Materials

Acrylamide (AAm), 2-hydroxyethyl methacrylate (HEMA), 1-pyrenylbutyric acid, 1-(3-dimethylaminopropyl)-3-ethylcarbodiimide hydrochloride (EDC·HCl), 4-dimethylaminopyridine (DMAP), and sodium chloride (NaCl) were purchased from Sinopharm Chemical Reagent Co., Ltd. (Shanghai, China). Allylamine, sodium alginate (Alg), *N*,*N*′-methylene bis(acrylamide) (BIS), $CH_2Cl_2$, APS, TEMED, calcium chloride ($CaCl_2$), gelatin, polyvinyl alcohol (PVA), ferroferric oxide ($Fe_3O_4$), rhodamine B, congo red, methyl violet, methyl blue, tartrazine, xylenol orange sodium salt (XO), ammonium ferrous

**DOI:** 10.31635/ccschem.022.202201942
**Citation:** *CCS Chem.* **2023**, 5, 704–717
**Link to VoR:** https://doi.org/10.31635/ccschem.022.202201942

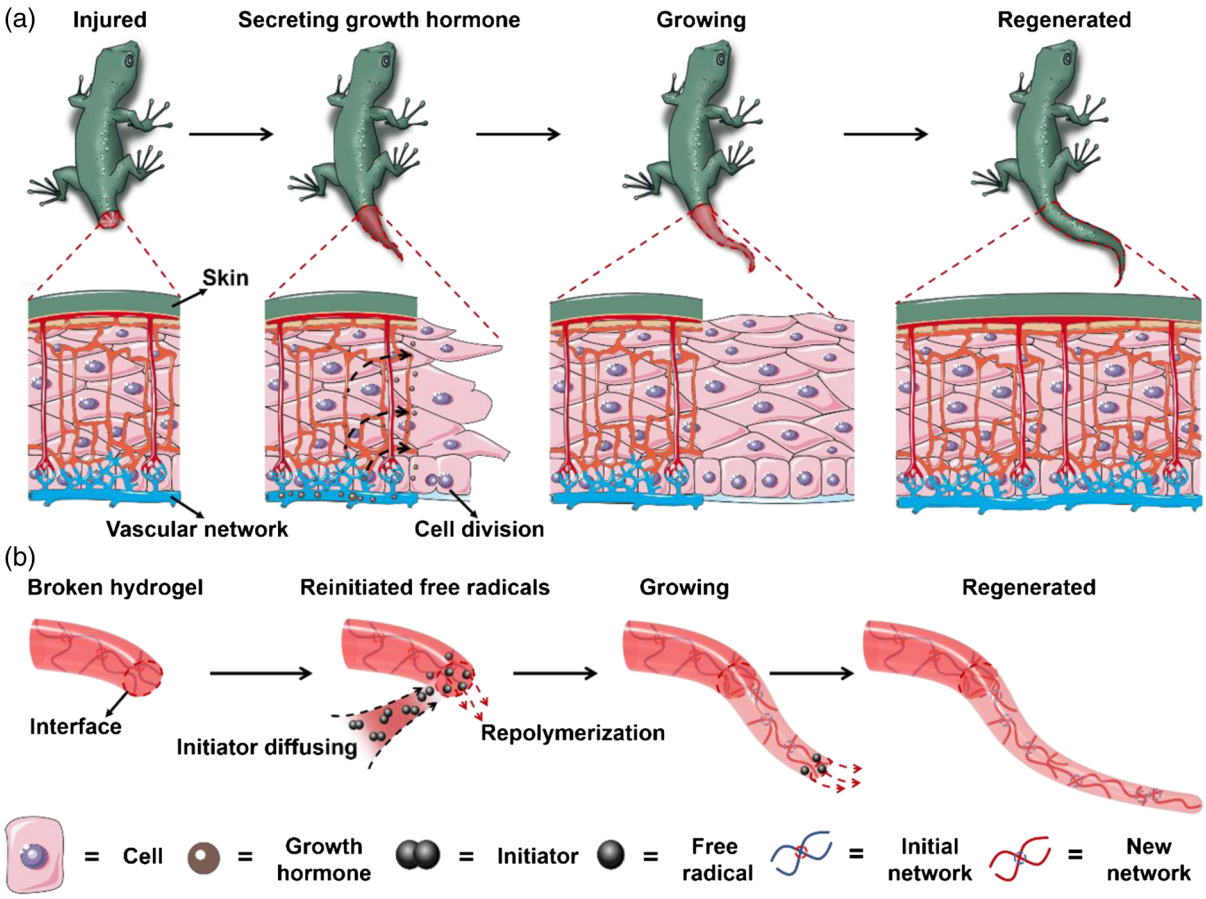


**Scheme 1** | *Gecko-inspired regeneration of polymeric hydrogels. (a) The typical regeneration process of severed gecko tails. The injured gecko would secrete and transport growth hormone which induces the division of cells in the injured part and regenerates until the injured part is recovered. (b) Gecko-inspired hydrogel-regenerating strategy. The free radicals were reinitiated at the solid–liquid interface and induced the polymerization in order to reconstruct the new hydrogel network.*

sulfate ($Fe(NH_4)_2{\cdot}(SO_4)_2{\cdot}6H_2O$), and ethylene diamine tetraacetic acid (EDTA) were purchased from Aladdin Reagent Co., Ltd. (Shanghai, China). *N*-hydroxyethyl acrylamide (HEAA), and *N*-isopropylacrylamide (NIPAm) were purchased from TCI Reagent Co., Ltd. (Shanghai, China). 4-Bromo-1,8-naphthalicanhydrideand, and *N,N′*-dimethylethylenediamine were bought from Energy Chemical Co., Ltd. (Anhui, China).

## Instruments

The lyophilizing process was conducted in the DGJ-10C freeze dryer (Shanghai Boden Biological Science and Technology Co., Ltd., Shanghai, China). The tensile tests were conducted on the Z1 Zwick/Roell Universal Testing System (Shanghai Zwick Testing Equipment Technical Service Co., Ltd., Shanghai, China). Tensile tests were performed at room temperature with the tensile speed of 10 mm/min. Samples were punched into dumbbell shapes (size: length × width × thickness: 50 mm × 3 mm × 1 mm). The images and videos of hydrogel were taken by a polarizing microscope (OLYMPUS, 71781687-5, Japan). UV–vis absorption spectra were recorded by virtue of TU-1810 UV–vis spectrophotometer provided by Purkinje General Instrument Co., Ltd. (Beijing, China). The patterned hydrogels were obtained by laser cutter (GY-460 bought from Shandong Liaocheng Guangyue Laser Equipment Co., Ltd., Shandong, China).

## The fabrication of the substrate hydrogel

### *The fabrication of the substrate polyacrylamide hydrogel*

AAm (0.71 g), Bis (21.3 mg), APS (21.3 mg), TEMED (15 μL), and deionized water (10 mL) were mixed to form an aqueous solution. Then the hydrogel precursor was added into a 1 mm thick mold. The polymerization was carried out at room temperature for 6 h. After polymerization, the polyacrylamide (PAAm) hydrogel was

**DOI:** 10.31635/ccschem.022.202201942
**Citation:** *CCS Chem.* **2023**, 5, 704–717
**Link to VoR:** https://doi.org/10.31635/ccschem.022.202201942

immersed in deionized water to remove unreacted monomer and reach a swelling equilibrium.

### *Fabrication of the substrate PNIPAm hydrogel*

NIPAm (2 g), Bis (20 mg), APS (20 mg), TEMED (20 μL), and deionized water (10 mL) were mixed to form an aqueous solution. The hydrogel precursor solution was added into a 1 mm thick mold. The polymerization was carried out at 4 °C for 12 h. After polymerization, the PNIPAm hydrogel was immersed in deionized water to remove unreacted monomer and reach a swelling equilibrium.

### *Fabrication of the substrate polyvinyl alcohol hydrogel*

PVA was dissolved in deionized water (weight ration of PVA to $H_2O$ is 1:9) under an oil bath at 95 °C for 4 h to form an aqueous solution. The solution was added into a 1 mm thick mold. During the freezing/thawing treatment, the PVA solution was frozen under –18 °C for 6 h and thawed at room temperature for 2 h. The procedure was repeated three times in order to get PVA hydrogels.

### *Fabrication of the substrate gelatin hydrogel*

Gelatin was dissolved in deionized water (the weight ratio of gelatin to $H_2O$ was 3:20) under an oil bath at 60 °C for 1 h to form an aqueous solution. The solution was added into a 1 mm thick mold. The gelatinization process was carried out in a 4 °C environment.

### *Fabrication of the substrate Alg-$Ca^{2+}$ hydrogel*

Gelatin (15 g), $CaCl_2$ (1.11 g), and deionized water (100 mL) were mixed to form an aqueous solution at 60 °C in an oil bath, and the gelatin-$Ca^{2+}$ hydrogel was prepared using a similar procedure to prepare the gelatin hydrogel. Then 2% alginate solution was put on the top of gelatin-$Ca^{2+}$ hydrogel. After 10 min, the Alg-$Ca^{2+}$ hydrogel was obtained after transferring the gelatin/alginate hydrogel into warm water to remove the gelatin.

## The measurement of free radical concentration

PAAm hydrogel was selected as the substrate hydrogel in this experiment. The PAAm hydrogel was immersed in 15 mg/mL APS solution overnight. Then the hydrogel was removed, and the surface was dried.

The low viscosity precursor was prepared by mixing AAm (0.71 g), Bis (21.3 mg), I2959 (21.3 mg), $Fe(NH_4)_2{\cdot}(SO_4)_2{\cdot}6H_2O$ (0.196 g), and deionized water (10 mL). The high viscosity precursor was prepared by mixing linear polyacrylamide (0.71 g), AAm (0.71 g), Bis (21.3 mg), I2959 (21.3 mg), $Fe(NH_4)_2{\cdot}(SO_4)_2{\cdot}6H_2O$ (0.196 g), and deionized water (10 mL).

A PAAm hydrogel sheet (size: length × width × thickness: 40 mm × 10 mm × 1 mm) was first put into a homemade mold including one hollow silicone rubber sheet and two glass side pieces. Then the precursor was injected into the mold on top of the PAAm hydrogel. After 10 min, the hydrogel was irradiated under ultraviolet light (365 nm) for 5 min. The newly generated hydrogel was cut into strips 20 mm × 1 mm × 1 mm. An aqueous solution of 250 μM XO and 20 mM $H_2SO_4$ was used to determine the $Fe^{3+}$ content. After soaking the strips in 4.0 mL XO solution for 10 min, 3 mL solution was then taken from the test tube for UV–vis light analysis to determine the $Fe^{3+}$ concentration.

## The observation of interfacial diffusion polymerization

PAAm hydrogel was selected as the substrate hydrogel in this experiment. The PAAm hydrogel was immersed in 15 mg/mL APS solution overnight. Then the hydrogel was removed and the surface dried. The precursor was prepared by mixing linear polyacrylamide (0.71 g), AAm (0.71 g), Bis (21.3 mg), TEMED (150 μL), and deionized water (10 mL). A PAAm hydrogel sheet (size: length × width × thickness: 40 mm × 10 mm × 1 mm) was first put into a homemade molding including one hollow silicone rubber sheet and two glass side pieces. The model was placed on the stage of an optical microscope. Then the precursor was injected into the mold, and the generation of the new hydrogel was recorded and measured.

## The fabrication of hydrogel via interfacial diffusion polymerization

Some hydrophilic materials could be selected as the substrate, such as the PAAm hydrogel, gelatin hydrogel, calcium alginate hydrogel (Alg-$Ca^{2+}$ hydrogel), PVA hydrogel, paper, cloth, skin, fruit peel, and so on. All of the above hydrophilic substrates were immersed in 15 mg/mL APS solution overnight. The precursor was prepared by mixing polymers, monomer (1 M), crosslinking agent (3 wt % of monomer), dye, TEMED (15 μL/mL), and deionized water. For example, precursor 1 was prepared by mixing alginate (0.2 g), AAm (0.71 g), Bis (21.3 mg), TEMED (150 μL), and deionized water (10 mL) to form an aqueous solution. The precursor was coated on the surface of the substrate. After 30 min, a bilayer hydrogel was obtained after washing the ungelatinized precursor with deionized water.

A polydimethylsiloxane (PDMS) mold with a cutout pattern was placed on a substrate, and the precursor was placed on the top of the PDMS mold. After 30 min, a patterned hydrogel was obtained after washing the ungelatinized precursor with deionized water.

**DOI:** 10.31635/ccschem.022.202201942
**Citation:** *CCS Chem.* **2023**, 5, 704–717
**Link to VoR:** https://doi.org/10.31635/ccschem.022.202201942

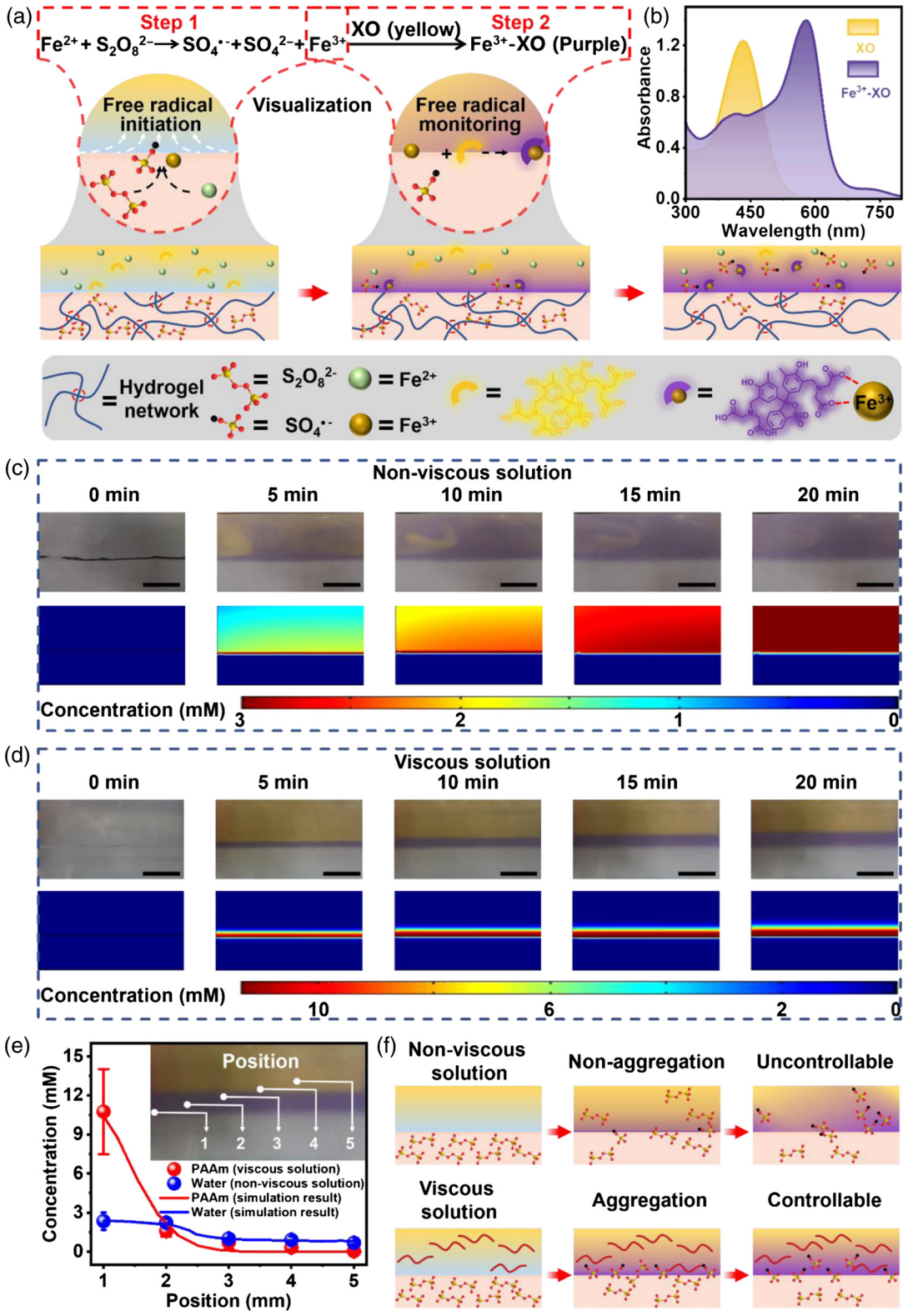


**Figure 1** | *Real-time monitoring of the diffusion of free radicals. (a) Schematic illustration of the generating and diffusing process of free radicals. (b) The UV absorption spectra of XO and $Fe^{3+}$-XO. (c) The images and finite element analysis simulation showing the diffusing process of free radicals in nonviscous solution. (d) The images and finite element analysis simulation showing the diffusing process of free radicals in viscous solution. (e) The experimental and simulation results of the concentration of free radicals in different positions. (f) The illustration showing the mechanism of regeneration and diffusion of free radicals. Scale bars: 1 cm.*

**DOI:** 10.31635/ccschem.022.202201942
**Citation:** *CCS Chem.* **2023**, 5, 704–717
**Link to VoR:** https://doi.org/10.31635/ccschem.022.202201942

### The process of hydrogel custom repair

During the fabrication and forthputting process, hydrogel actuator may face various types of damage that may destroy its function and interrupt the task in progress. In order to demonstrate this, various types of injury—such as piercing, cutting, and severing—were endowed to the two-dimensional butterfly-shaped hydrogel actuator. To custom repair the function of the hydrogel actuator, the injured part was treated with 15 mg/mL APS first. Then the hydrogel precursor containing AAm as monomer was utilized to repair the injured part of the bottom layer hydrogel (PAAm) via IDP. Subsequently, the AAm in the hydrogel precursor was replaced with NIPAm to repair the top layer hydrogel (PNIPAm) via IDP. Ultimately, all kinds of injuries were repaired, and the repaired hydrogel actuator was able to continue the incomplete task.

### Theoretical model

In order to describe the dynamic distribution process of free radicals in solution, the convection-diffusion control equation was adopted, and the expression is as follows:

$$\frac{\partial C_A}{\partial \tau}+u_x\frac{\partial C_A}{\partial x}+u_y\frac{\partial C_A}{\partial y}+u_z\frac{\partial C_A}{\partial z}=D_{AB}\left(\frac{\partial^2 C_A}{\partial x^2}+\frac{\partial^2 C_A}{\partial y^2}+\frac{\partial^2 C_A}{\partial z^2}\right)+r_A$$

In the above formula, $C_A$ represents the concentration of the diffusing substance component A, $u_x$, $u_y$, and $u_z$ represent the diffusion speed of the substance, respectively, $D_{AB}$ represents the diffusion coefficient of the diffusing substance A in B, and $r_A$ represents the amount of component A generated by chemical reaction in a unit volume of space per unit time. $\tau$ represents time, and $x$, $y$, and $z$ represent spatial coordinate positions. In this study, $C_A$ describes the concentration of the free radical components of the gel, and $D_{AB}$ represents the diffusion coefficient of the gel in the growth solution. Because the chemical reaction is considered, the growth solution is poured on the surface of the acrylamide hydrogel. APS in acrylamide will diffuse from the inside of the gel to the growth solution. APS will react with $Fe^{2+}$. Therefore, $r_A$ is determined by the following chemical reaction equation:

$$Fe^{2+}+S_2O_8^{2-}\rightarrow SO_4^{\bullet-}+SO_4^{2-}+Fe^{3+}\xrightarrow{XO(yellow)}Fe^{3+}-XO(Purple)$$

The finite element method was processed by *Transport of Diluted Species* (TDS). The initial parameters were defined as follows: the initial concentration of $S_2O_8^{2-}$ was 15 mg/mL and the initial concentration of $Fe^{2+}$ in the hydrogel precursor was 100 mM. The definition of the boundary condition parameters: the bottom and two sides were set as closed boundaries (No Flux), and the top boundary was set as an open boundary (Open Boundary). The diffusion coefficient values were set as $3*10^{-7}$ $m^2/s$ in the viscous solution and $2*10^{-10}$ $m^2/s$ in the viscous solution (where the viscous growth solution contained 100 mM $Fe^{2+}$, 20 mM xylenol orange (color indicator), and 1M linear polyacrylamide.

The above chemical reaction processes were defined via the *Chemistry* (chem) module. The reacting substances and the generated substances were in a one-to-one correspondence with the four diffusing substances in the TDS module since the reaction was irreversible. The reaction rate $r_A$ parameter, the amount of chemical reaction generated in a unit volume of space per unit time, was jointly determined by the forward rate constant of the reactants $Fe^{2+}$ and $S_2O_8^{2-}$ and defined by default in the software. Additionally, the *Enthalpy of reaction* and *Entropy of reaction* adopted the definition of Automatic. Finally, the reaction rates of each substance were coupled into the TDS module, and they affected the diffusion of the generated substances.

## Results and Discussion

As is well known, the generation of free radicals is the key step in free radical polymerization. Therefore, in order to clarify the mechanism of the polymerization process of IDP, the as-prepared hydrogel was immersed into the solution of initiators (APS), and the initiators diffused into the hydrogel network until they reached equilibrium. Then, a solution containing $Fe^{2+}$ as a reduction agent and xylenol orange (XO) as indicator of $Fe^{3+}$ formation was poured onto the surface of the initial hydrogel to monitor the generation and diffusion process of free radicals (Figure 1a). The generation and monitoring process of free radicals can be described as follows. Due to the osmotic pressure at the solid–liquid interface, initiator molecules diffused from the hydrogel network into solution while the $Fe^{2+}$ diffused from the solution into the hydrogel, which triggered the redox reaction and generated $Fe^{3+}$ and free radicals. As soon as redox initiation occurred, the Fenton color reaction set in and resulted in a color change from yellow to purple, due to the metal coordination between XO and $Fe^{3+}$ (Figure 1b). With the ongoing diffusion of APS, $Fe^{2+}$ ions were further oxidized into $Fe^{3+}$, and the color of the solution gradually changed from yellow to purple.

When the viscosity of the solution was low, the diffusion rate was fast, and a large number of unreacted APS escaped from the interface and made the generation process of free radicals uncontrollable (Figure 1c and Supporting Information Movie S1). Therefore, to slow the diffusion rate of APS, polyacrylamide (PAAm) was dissolved into the solution in order to increase the viscosity of the solution. With the increased viscosity of the solution, the diffusion rate of APS slowed down. In consequence, the generation process of free radicals became more controllable, and a clear dividing line between reacted and unreacted parts

**DOI:** 10.31635/ccschem.022.202201942
**Citation:** *CCS Chem.* **2023**, 5, 704–717
**Link to VoR:** https://doi.org/10.31635/ccschem.022.202201942

was observed and moved slowly forward by the diffusion of APS (Figure 1d and Supporting Information Movie S2). Further, the diffusing process of APS and the generating process of free radicals were simulated by finite element modeling, and the results are highly consistent with the experimental results.

It is worth noting that the number of free radicals is equal to that of $Fe^{3+}$ ions, and thus accurately measuring the concentration of $Fe^{3+}$ ions allows for estimation of the concentration of free radicals. Therefore, the concentration of $Fe^{3+}$ ions was determined by UV–vis light absorption spectroscopic analysis (Supporting Information Figure S1), and the corresponding concentration of free radicals was calculated. As shown in Figure 1e, there was an unclear gradient distribution of free radicals when using a low-viscous solution with the concentration of free radicals was 2.35 mM in position 1 and 0.68 mM in position 5. In contrast, in a viscous solution, the concentration of free radicals increased to 10.75 mM in position 1 while the concentration of free radicals decreased by two orders of magnitude to 0.04 mM in position 5. With the assistance of finite element analysis, the diffusing mechanism was furtherly clarified (Supporting Information Figure S2). In the low viscosity solution, the diffusion of APS experienced less resistance, resulting in less APS gathering at the solid–liquid interface, which induced a low free radical initiation rate on the one hand. Hence, more unreacted APS quickly diffused further into the solution, which generated free radicals far from the interface on the other hand. However, in the solution with higher viscosity, the diffusing process of APS was restricted by the polymer chains inside the solution (Figure 1f). Therefore, more APS gathered at the solid–liquid interface, which induced a fast initiation rate of free radicals due to the high concentration of APS. Consequently, much less APS escaped into the solution, resulting in a clear gradient distribution of free radicals.

As mentioned above, the use of a high-viscosity solution effectively affected the generation process and diffusion rate of free radicals, making the polymerization more controllable. This motivated us to introduce the IDP strategy to the fabrication of hydrogels. Also, in order to enrich the function of the new hydrogel, a hydrogel precursor containing AAm as monomer, TEMED as reduction agent, Bis as crosslinker, and alginate as thickener was introduced onto the surface of an APS-doped hydrogel. As shown in Figure 2a, the initiator diffused from the hydrogel into the solution while AAm and Bis diffused from the solution into the hydrogel network because of the osmotic pressure at the solid–liquid interface. Thus, a large number of free radicals was generated via redox initiation with APS and TEMED, which triggered the process of gelation at this location. Finally, a new hydrogel was formed and gradually grew on the top of the initial hydrogel. Compared with the traditional fabrication, IDP strategy generated free radicals within the solid–liquid interface, so the newly formed hydrogel network interpenetrated into the initial hydrogel network and formed an interpenetrating network at the interfacial area (Figure 2b). Within the gelation process, optical refraction occurred on the boundary between the gelled part and the nongelled part, which can be distinguished as a dark line when observed with an optical microscope. Therefore, with the assistance of an optical microscope, the self-growth process the new hydrogel was monitored in real time (Supporting Information Figure S3). This clearly showed that the new hydrogel grew to the thickness of 1 mm within 5 min (Figure 2c).

It is worth noting that the Alg, which was utilized as a thickener, played an essential part during the growing process of the new hydrogel. With the concentration of Alg increased from 0 % to 2%, the corresponding viscosity of the solution increased from 0 to 0.468 Pa·s (Supporting Information Figure S4). When Alg was eliminated completely from the hydrogel precursor, the gelation became uncontrollable due to the fast and random diffusion of free radicals, and the boundary between the gelled and nongelled parts rapidly forwarded in a short time (Supporting Information Figure S5 and Movie S3), which means that the new hydrogel cannot be obtained on the surface of the initial hydrogel.

Similarly, when the viscosity of precursor was low (the concentration of alg <0.1%), a similar phenomenon in which the thickness of new hydrogel is 0.68 mm at 1 min and 0.71 mm at 5 min was observed (Figure 2d). But, with the increase of the viscosity, the growth process was gradually improved. When the concentration of alg (thickener) increased above 0.1%, the thickness of new hydrogel grew from 0.41 mm at 1 min to 0.94 mm at 5 min. Besides, when the concentration of alg further increased to 2%, the thickness decreased to 0.32 mm after 1 min but increased to 1.05 after 5 min (Supporting Information Movie S4) because the diffusion rate of free radicals was slowed down by the high concentration of alg, which induced the high gradient distribution of free radicals. In this case, the factor that determined the growth rate was no longer the generation of free radicals but the chain growth reaction. As mentioned above, although the diffusion of initiators was also slowed down by increasing the crosslinking density of the hydrogel substrate, the diffusion process in the hydrogel precursor was not affected. Thus, slowing down the diffusion of initiator in the hydrogel precursor is necessary for IDP. It is worth noting that the maximum growth thickness of new hydrogel was limited by the loss of free radicals during the diffusing and polymerizing process. Thus, the thickness of new hydrogel increased to 2.7 mm in 1 h (Supporting Information Figure S6).

Subsequently, the effect of the concentration of initiators and monomers was also explored. As shown in Figure 2e, with the increasing concentration of APS, the number of generated free radicals increased rapidly,

**DOI:** 10.31635/ccschem.022.202201942
**Citation:** *CCS Chem.* **2023**, 5, 704–717
**Link to VoR:** https://doi.org/10.31635/ccschem.022.202201942

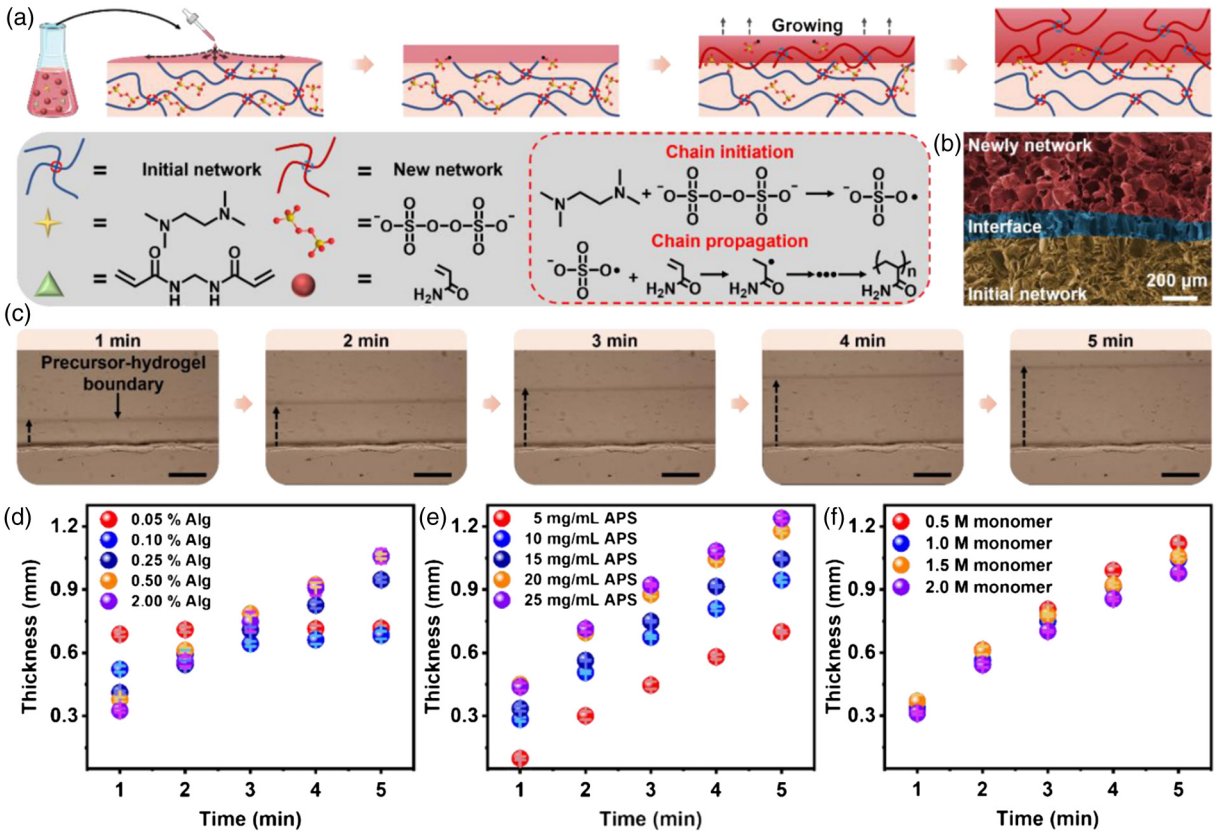


**Figure 2** | *Real-time monitoring of the growing process of new hydrogels upon the initial hydrogel layer. (a) Schematic illustration of the hydrogel growing process. The hydrogel precursor was placed on the surface of initial hydrogel and a new hydrogel grow via IDP. (b) The cross-section SEM images of the bilayer hydrogel where the new hydrogels grow on the surface of initial hydrogel. (c) Images showing the real-time monitoring of growing process. (d) The growth kinetic curve with different concentrations of Alg. (e) The growth kinetic curve with different concentrations of APS. (f) The growth kinetic curve with different concentrations of monomer. Scale bars: 0.5 mm.*

which resulted in a stronger osmotic pressure and further increased the growth kinetics. Different from the effect of concentration of APS, when the concentration of monomers was increased (Figure 2f), although the kinetics of polymerization also increased, the density of the new hydrogel network also increased, hindering the diffusion of free radicals and slightly reducing the growth rate. It is worth noting that the IDP strategy can also utilize the polymerization of other monomers such as HEAA and NIPAm. In this situation, the growth kinetics were determined by the monomer reactivity (Supporting Information Figure S7).

With the assistance of a patterned mask, the shape of new hydrogel that grew from the surface of the initial hydrogel was precisely designed. As shown in Figure 3a, a star-shaped mask was placed on the surface of a PAAm hydrogel containing APS, and the hydrogel precursor was dropped on the cavity of the star-shaped mask. Subsequently, a new hydrogel with a star shape grew gradually via IDP. In order to evaluate the microscopic morphology of the new hydrogel, the star-shaped hydrogel was observed by a confocal laser scanning microscope. As shown in Figure 3b, within the 2500 × 2500 μm scanning plane, the image of a star shape was clearly captured, which indicated that the growth plane was parallel to the substrate, and the new hydrogel grew along the direction perpendicular to the plane. Further, the growth height of every 1 mm distance of star-shaped hydrogel was measured. All showed a flat surface, and the height of the hydrogel decreased from the center of the star to the edge of the star, which could be caused by the polymerization inhibition of the PDMS mask (Figure 3c). Also, when the hydrogel precursor was removed during the growth process, the new hydrogel with a designed height was obtained (Figure 3d). Therefore, inspired by the growth after releasing the mask, a visually intermingled hydrogel array was prepared, where the templated part of the hydrogel array was allowed to grow higher than the other parts. By changing the predesign masks, diverse patterns can be prepared on the surface of a hydrogel substrate in the shape of a letter, such as “C,” “A,” or “S” (Figure 3e). More interestingly, patterns can also grow on the curved

**DOI:** 10.31635/ccschem.022.202201942
**Citation:** *CCS Chem.* **2023**, 5, 704–717
**Link to VoR:** https://doi.org/10.31635/ccschem.022.202201942

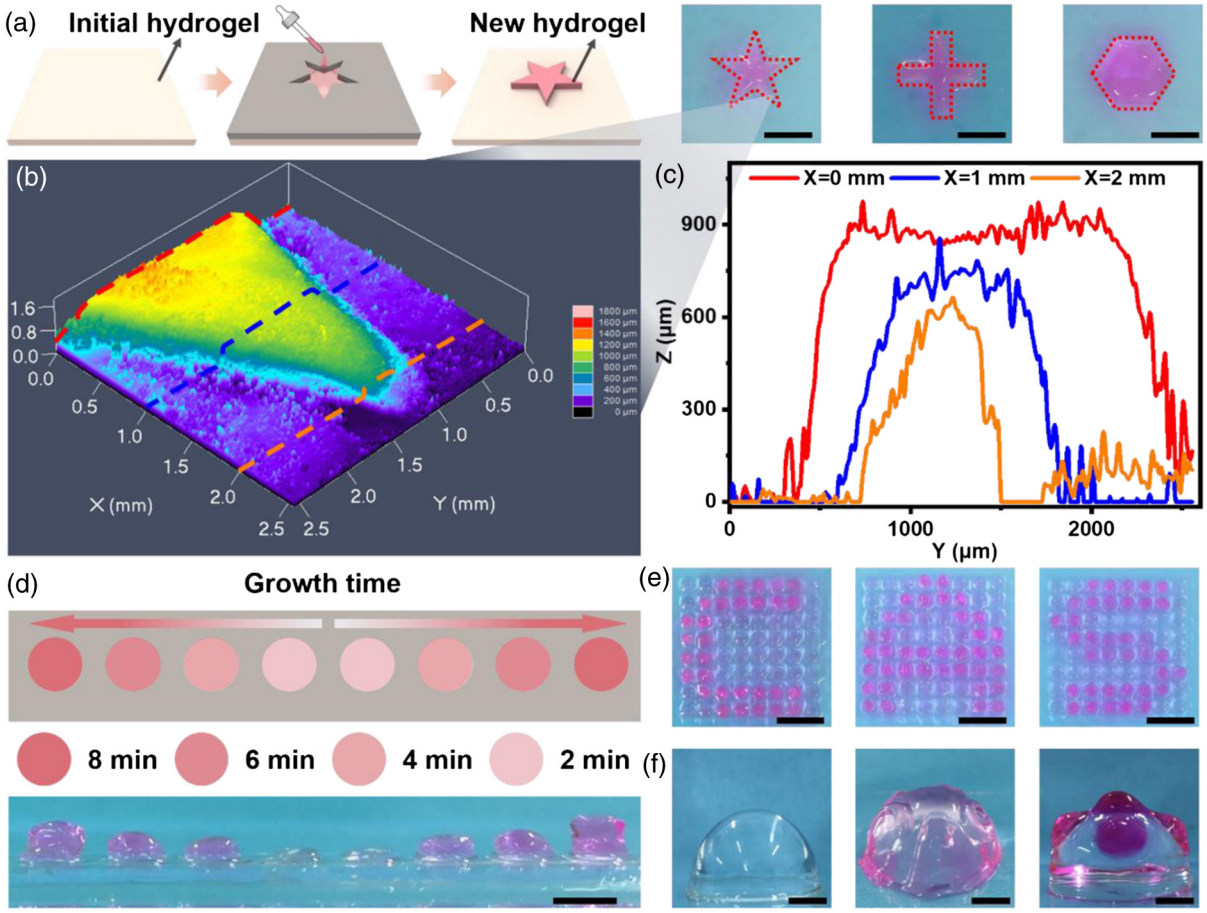


**Figure 3** | *The regulation of the shape of new hydrogel. (a) Illustration and images showing the precise design of the shape of new hydrogel with the assistance of a patterned mask. (b) The image of confocal laser scanning microscope showing the microscopic morphology of new hydrogel. (c) The profile of the grown structure obtained in different positions. (d) The height of new hydrogel in different growth times. (e) The images showing the visually intermingled hydrogel array. (f) The images showing the 3D hydrogel hemisphere with various patterns. Scale bars: 1 cm.*

surface of a hemispheric hydrogel by controlling the distribution of APS. Additionally, a strange hydrogel hemisphere with various small spheres grew on the surface of a big sphere in the same way (Figure 3f and Supporting Information Figure S8).

As discussed above, IDP is based on three principles: (1) The oxidant (APS) and reducer (TEMED or $Fe^{2+}$) should be separated and placed into a solid substrate and a liquid solution, respectively. (2) The substrate should be hydrophilic and contain the oxidant. (3) The hydrogel precursor must be a viscous solution. The first principle is obvious. Therefore, the approach of IDP is a universality strategy as long as it satisfies the second and third principles. For example, a gelatin substrate containing APS also meets the second principle, and the viscous hydrogel precursor including thickener and hydrophilic dyes conforms to the third principle. Thus, a new hydrogel grew from the gelatin via IDP. Further, with the assistance of a patterned mask, a multicolor hydrogel was fabricated on the surface of the gelatin platform, utilizing various hydrogel precursors containing different dyes (Figure 4a). In order to further prove the universality of IDP, many different types of hydrogel platforms were prepared by normal polymerization (PAAm hydrogel), hydrogen bonds (gelatin), metal-ligand coordination (Alg-$Ca^{2+}$ hydrogel), and crystalline aggregate (PVA hydrogel). The corresponding patterned hydrogels were obtained in different shapes such as the moon, a fish, the sun, and a bird (Figure 4b). Subsequently, the growth rates of hydrogel on different hydrogel-based substrates were investigated, and all of the newly formed hydrogels achieved the thickness of about 1 mm within 5 min (Figure 4c), indicating that hydrogels effectively grew on all of the hydrogel-based substrates via IDP.

Using fluorescent polymers in the mixture, as well as homopolymers and copolymers as thickener to increase the viscosity of hydrogel precursors, hydrogels with fluorescent properties were successfully formed on the surface of substrates via IDP (Figure 4d). For instance, rhodamine B, an orange fluorescent molecule, was

**DOI:** 10.31635/ccschem.022.202201942
**Citation:** *CCS Chem.* **2023**, 5, 704–717
**Link to VoR:** https://doi.org/10.31635/ccschem.022.202201942

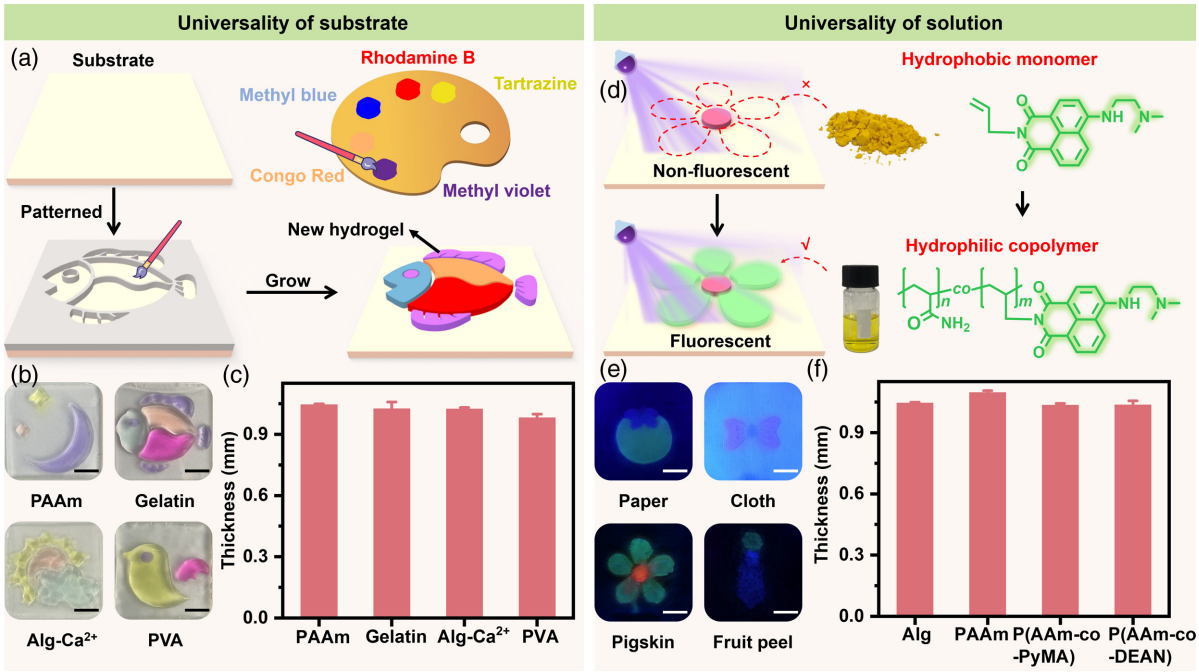


**Figure 4** | *The universality of the IDP strategy. (a) Schematic illustration of the fabrication process of multicolor hydrogel on hydrogel substrates via IDP. (b) Images showing the multicolor hydrogels on various kinds of hydrogel substrates. (c) The thickness of new hydrogel which grow on various kinds of hydrogel substrates in 5 min. (d) Schematic illustration of the fabrication process of fluorescent hydrogel via IDP. (e) Images showing the fluorescent property of hydrogel grown in various hydrophilic substrates. (f) The thickness of new hydrogels which use various kinds of polymers as a thickener in 5 min. Scale bars: 1 cm.*

mixed with Alg to prepare an Alg/ rhodamine B mixture. 1-Pyrenylmethyl acrylate (PyMA), a blue fluorescence monomer, was copolymerized with AAm to prepare P(AAm-co-PyMA). Similarly, 4-(*N*,*N*-dimethylaminoethylene) amino-*N*-allyl-1,8-naphthalimide (DEAN), a yellow-green fluorescence monomer, was copolymerized with AAm to prepare PAAm-co-PDEAN. According to the second and third principles, Alg/rhodamine B mixture, P(AAm-co-PyMA), and P(AAm-co-DEAN) increased the viscosity of hydrogel precursors and fabricated corresponding fluorescence hydrogels on hydrophilic substrates (Supporting Information Figure S9). As shown in Figure 4e, with the assistance of a patterned mask, various fluorescent patterns such as an apple, a cravat, a flower and a necktie were encoded on the surface of natural products such as paper, cloth, pigskin, and fruit peel. Finally, the growth rate of hydrogels with different thickeners was also measured (Figure 4f), and all of the hydrogels could grow to the thickness of 1 mm within 5 min, which further proves that the IDP strategy is a universal strategy. Therefore, new performance can be endowed via the IDP strategy by choosing functional thickeners.

Wound repair, one of the most fantastic properties of biological organisms, enables biological organisms to rebuild their structure and recover their function. For example, when our fingers are pierced, blood flows out and immediately forms a scab. Then, the cells in the boundary area of the injury quickly divides and gradually fill up the injured cavity from the inside out. Herein, an "injured" hydrogel is expected to regenerate the damaged part via IDP. Inspired by the inside-out repair process of biological organisms, APS was introduced into an injured hydrogel network by penetration. Then, the hydrogel precursor solution was poured into the injured part. Finally, a new hydrogel network was rebuilt in the area of the injured part via IDP (Supporting Information Figure S10). Further, even if the hydrogel suffered serious damage, the wound could be repaired in the same way (Supporting Information Figure S11). Moreover, even if the hydrogel was totally disconnected, the hydrogel could be repaired via IDP. As shown in Supporting Information Figure S12, a rectangular hydrogel containing APS, was cut into two blocks, and the hydrogel precursor solution was injected into the cavity between the two hydrogel blocks. Then, due to the osmotic pressure, the initiator diffused from the injured hydrogel to the hydrogel precursor while the monomer diffused from hydrogel precursor to the injured hydrogel, triggering polymerization in the interface and generating a lot of

**DOI:** 10.31635/ccschem.022.202201942
**Citation:** *CCS Chem.* **2023**, 5, 704–717
**Link to VoR:** https://doi.org/10.31635/ccschem.022.202201942

polymer chains. On the one side, the newly generated polymer chains entangled with the injured hydrogel network and formed stable physical entanglements. On the other side, the new hydrogel grew toward the precursor and formed stable covalent bonding. Therefore, the two disconnected hydrogels were reconnected to form a complete hydrogel. Besides, no matter how the hydrogel was cut, the two hydrogel parts were able to be reconnected by the newly formed hydrogel and exhibited similar mechanical properties as before (Supporting Information Figure S13 and Movie S5).

Subsequently, the mechanical properties of the hydrogel before and after the repair process have been evaluated. As shown in Supporting Information Figure S14, the maximum stress of the original hydrogel is 49 kPa, and the maximum strain is 137%. When the injured hydrogel was repaired by a viscous precursor containing 1 M monomer, the maximum fracture stress recovered to 8.9 kPa. Furthermore, when the concentration of monomer in the hydrogel precursor increased to 3 M, the maximum fracture stress increased to 49.5 kPa, and the maximum strain was 129% which indicates that the injured hydrogel was repaired to the original state. In fact, when the concentration of monomer further increased to 5M, more physical entanglements was generated. and the repaired hydrogel was broken in a new position instead of the repaired area, which means that the adherent stress was stronger than the original hydrogel. Relatively, when the nonviscous hydrogel precursor was utilized to repair the injured hydrogel, the adherent property is much worse than the viscous hydrogel precursor since the inferior interfacial polymerization and entanglements (Supporting Information Figure S15), which indicated that the viscosity of hydrogel precursor not only determines the growth process of the new hydrogel but also influences interfacial interaction.

Inspired by the tail-regenerating ability of geckos, when some part of a hydrogel was totally lost, the injured hydrogel could be regenerated via IDP. As shown in Supporting Information Figure S16, the top part of the starfish-shaped hydrogel was cut off. Then, the remaining part was immersed into the solution of APS, and the hydrogel precursor was placed on the surface of the injured part with the assistance of a tubular mold. After several alternating treatments of APS and the hydrogel precursor, a new part of the starfish-shaped hydrogel was gradually regenerated.

Usually, a typical PAAm hydrogel cannot respond to an external stimulus such as heat, light, or pH, and both the chemical components and the macrostructures cannot be changed once formed. However, by selecting stimuli-responsive monomers and introducing them into the hydrogel precursor solution, a new stimuli-responsive hydrogel can grow on the surface of an initially passive hydrogel (PAAm) via IDP. As shown in Supporting Information Figure S17, a six claw-shaped blue fluorescent hydrogel (PAAm/P(AAm-*co*-PyMA)) was first prepared. Then, a hydrogel precursor solution containing NIPAm as monomer and P(AAm-*co*-DEAN) as thickener was placed onto the surface of PAAm/P(AAm-*co*-PyMA) hydrogel, and the new hydrogel (PNIPAm/P(AAm-*co*-DEAN)) with thermoresponsive and yellow-green fluorescent properties grew on the surface of initial hydrogel. Due to the thermoresponsive property of PNIPAm, the bilayer hydrogel could self-deform in hot water and recover in cold water (Supporting Information Figure S17II–III). In addition, the inert hydrogel was endowed with a shape memory property in the same way. For example, a hydrogel precursor solution containing AAm as monomer, Alg as a thickener, and rhodamine B as a fluorescent molecule was placed onto the surface of PAAm/P(AAm-co-PyMA) hydrogel to grow Alg/PAAm hydrogel. Due to the $Ca^{2+}$-Alg coordination, the bilayer hydrogel could fix the three-dimensional temporary shape and recover the two-dimensional original shape by EDTA (Supporting Information Figure S17IV–V). These results indicate that both the chemical components and macrostructures can be endowed and encoded via IDP.

Moreover, lost functionalities of hydrogels were regenerated via IDP. As shown in Figure 5, a six claw-shaped hydrogel actuator lost one claw with an actuating property and one claw with a shape memory property. Under traditional conditions, the injured actuator could not be used again. But now, the injured part of the hydrogel actuator could be regenerated via IDP. For instance, hydrogel precursor solution containing AAm as monomer and P(AAm-*co*-PyMA) as thickener was utilized to grow new claws from the injured part of the initial hydrogel. Then, hydrogel precursor containing NIPAM or Alg were utilized to repair the functions of actuating and shape memory, respectively (Supporting Information Figure S18). Finally, the injured hydrogel actuator was regenerated and exhibited the same condition and functions as before (Supporting Information Movie S6). In addition, a hydrogel actuator suffering from various types of damage such as piercing, cutting, and severing, could be repaired completely, and the hydrogel actuators could deform as before (Supporting Information Figure S19).

## Conclusion

In summary, inspired by the tail regeneration of the gecko, we reported an efficient and universal strategy of an IDP to regenerate the polymeric hydrogel at a solid–liquid interface, thereby regrowing new hydrogels on the surface of existing hydrogels. In this strategy, the initiator was firstly introduced into an existing hydroge. Hydrogel precursor solution containing accelerator and monomers was then put on the surface of the above hydrogel, which

**DOI:** 10.31635/ccschem.022.202201942
**Citation:** *CCS Chem.* **2023**, 5, 704–717
**Link to VoR:** https://doi.org/10.31635/ccschem.022.202201942

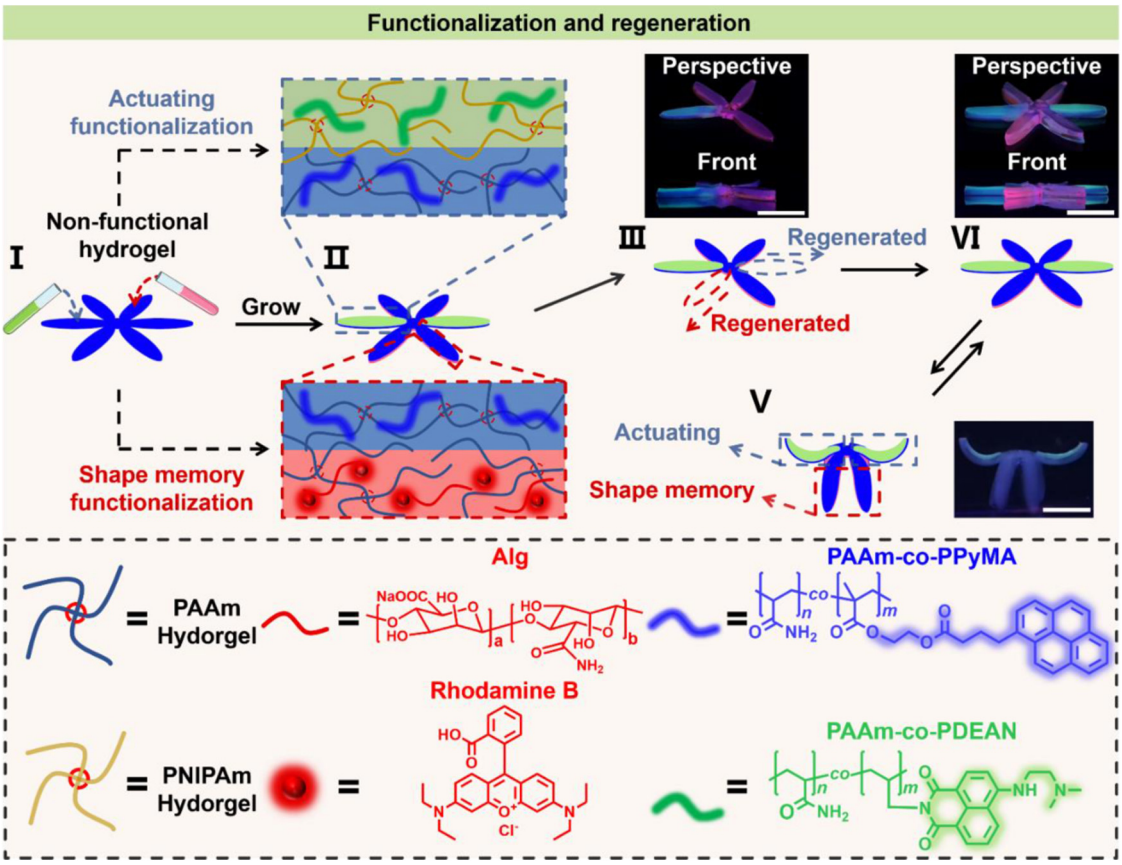


**Figure 5** | *Hydrogel functionalization and regeneration process via IDP. (I) Illustration of initial hydrogel substrate. (II) Process of the shape memory and actuating functionalization: the hydrogel precursor containing AAm as monomer and Alg as thickener was placed onto the surface of initial hydrogel to prepare shape memory hydrogel. The hydrogel precursor containing NIPAm as monomer was placed onto the surface of initial hydrogel to prepare bilayer hydrogel actuator. (III) The blue fluorescent substrate hydrogel was regenerated by hydrogel precursor containing AAm as monomer and PAAm-co-PPyMA as thickener first. Then, the actuating property was regenerated by hydrogel precursor containing NIPAm as monomer, and shape memory layer was regenerated by hydrogel precursor containing Alg as thickener. (IV and V) The shape memory and actuating process of regenerated hydrogel actuator. The hydrogel actuator was deformed by external force and the temporary shape fixed by 0.1 M $Ca^{2+}$ first. Then the hydrogel actuator could self-deform to three-dimensional shape in water of 60 °C. Scale bars: 1 cm.*

resulted in a redox initiation providing free radicals at room temperature. When the initiator diffused from the hydrogel and encountered to the accelerator, a new hydrogel network can be achieved on the surface of the initial hydrogel network. The hydrogel growth process can be controlled by adjusting the viscosity of the hydrogel precursor solution. The chemical structure of the newly formed hydrogel network can be tuned by changing the monomer and thickener of the hydrogel precursor solution, and diverse substrates such as hydrogels and hydrophilic surfaces were applied to grow new hydrogels. More importantly, the IDP strategy can be utilized to regenerate the injured part of a hydrogel and exhibit the same condition both in chemical structure and actuating property as before. We believe that our successful method can drive the development of many essential applications in the fabrication and regeneration of hydrogel actuators, soft robots, and bionic devices.

## Supporting Information

Supporting Information is available and includes standard curve of the concentration of $Fe^{3+}$; finite element analysis of the diffusion of APS; the monitoring of hydrogel growing process; the viscosity of Alg with different concentration; the growing process of hydrogel; the growth kinetic curves with different kinds of monomers; images of new hydrogels under natural light; the wound repair process of injured hydrogel; the tissue regenerating process of injured hydrogel; the monitoring of hydrogel repair process; the functional regeneration process of hydrogel and the images showing the custom repair of

**DOI:** 10.31635/ccschem.022.202201942
**Citation:** *CCS Chem.* **2023**, 5, 704–717
**Link to VoR:** https://doi.org/10.31635/ccschem.022.202201942

hydrogel. The diffusing process of free radicals in nonviscous solution (Movie S1). The diffusing process of free radicals in viscous solution (Movie S2). The growing process of hydrogel in nonviscous solution (Movie S3). The growing process of hydrogel in viscous solution (Movie S4). The stretching and twisting process of hydrogel after repairing (Movie S5). The complex shape deformation process of hydrogel actuator with shape memory and actuating properties (Movie S6).

## Conflict of Interest

The authors declare no competing financial interest.

## Funding Information

The National Natural Science Foundation of China (grant nos. 51873223 and 52073295), the Key Research Program of Frontier Science, Chinese Academy of Sciences (grant no. QYZDB-SSW-SLH036), the China Postdoctoral Science Foundation (grant no. 2020M671828), the Sino-German Mobility Programme (grant no. M-0424), and the K.C. Wong Education Foundation (grant no. GJTD-2019-13). The authors acknowledge the financial support of the Helmholtz Association.

## Acknowledgments

The authors acknowledge M.S. Dingyao Lai for helping draw the images of the gecko.

## References

1. Rao, P.; Sun, T. L.; Chen, L.; Takahashi, R.; Shinohara, G.; Guo, H.; King, D. R.; Kurokawa, T.; Gong, J. P. Tough Hydrogels with Fast, Strong, and Reversible Underwater Adhesion Based on a Multiscale Design. *Adv. Mater.* **2018**, *30*, 1801884.
2. Zhuo, S.; Zhao, Z.; Xie, Z.; Hao, Y.; Xu, Y.; Zhao, T.; Li, H.; Knubben, E. M.; Wen, L.; Jiang, L.; Liu, M. J. Complex Multiphase Organohydrogels with Programmable Mechanics toward Adaptive Soft-Matter Machines. *Sci. Adv.* **2020**, *6*, eaax1464.
3. Zhao, Z.; Zhang, K.; Liu, Y.; Zhou, J.; Liu, M. Highly Stretchable, Shape Memory Organohydrogels Using Phase-Transition Microinclusions. *Adv. Mater.* **2017**, *29*, 1701695.
4. Fan, H.; Gong, J. P. Fabrication of Bioinspired Hydrogels: Challenges and Opportunities. *Macromolecules* **2020**, *53*, 2769–2782.
5. Zhao, Y. S.; Lo, C. Y.; Ruan, L. C.; Pi, C. H.; Kim, C.; Alsaid, Y.; Frenkel, I.; Rico, R.; Tsao, T. C.; He, X. M. Somatosensory Actuator Based on Stretchable Conductive Photothermally Responsive Hydrogel. *Sci. Robot.* **2021**, *6*, eabd5483.
6. Wang, X.; Yang, B. S.; Tan, D.; Li, Q.; Song, B.; Wu, Z. S.; del Campo, A.; Kappl, M.; Wang, Z.; Gorb, S. N.; Liu, S.; Xue, L. J. Bioinspired Footed Soft Robot with Unidirectional All-Terrain Mobility. *Mater. Today* **2020**, *35*, 42–49.
7. Wang, R.; Shen, Y. N.; Qian, D.; Sun, J. K.; Zhou, X.; Wang, W. C.; Liu, Z. F. Tensile and Torsional Elastomer Fiber Artificial Muscle by Entropic Elasticity with Thermo-Piezoresistive Sensing of Strain and Rotation by a Single Electric Signal. *Mater. Horiz.* **2020**, *7*, 3305–3315.
8. Wang, Z. H.; Lin, B. X.; Sheng, S. Y.; Tan, S. C.; Wang, P. C.; Tao, Y.; Liu, Z.; He, Z. Y.; Wang, J. J.; Bioinspired Anti-Icing Hydrogel Enabled by Ice-Nucleating Protein. *CCS Chem.* **2022**, *4*, 104–111.
9. Hao, X.; Wang, H. R.; Zhao, W. J.; Wang, L. T.; Peng, F.; Yan, Q. Dynamic Macro- and Microgels Driven by Adenosine Triphosphate-Fueled Competitive Host-Guest Interaction. *CCS Chem.* **2021**, *3*, 1267–1275.
10. Le, X. X.; Lu, W.; Zhang, J. W.; Chen, T. Recent Progress in Biomimetic Anisotropic Hydrogel Actuators. *Adv. Sci.* **2019**, *6*, 1801584.
11. Wu, B. Y.; Lu, H. H.; Le, X. X.; Lu, W.; Zhang, J. W.; Théato, P.; Chen, T. Recent Progress in the Shape Deformation of Polymeric Hydrogels from Memory to Actuation. *Chem. Sci.* **2021**, *12*, 6472–6487.
12. Kempaiah, R.; Nie, Z. H. From Nature to Synthetic Systems: Shape Transformation in Soft Materials. *J. Mater. Chem. B* **2014**, *2*, 2357–2368.
13. Wang, Y. T.; Yuan, J.; Zhao, Y. P.; Wang, L.; Guo, L. X.; Feng, L.; Cui, J. W. Water-in-Water Emulsions, Ultralow Interfacial Tension, and Biolubrication. *CCS Chem.* **2021**, *3*, 2275–2287.
14. Fu, L. L.; Wang, H.; Li, H. B. Harvesting Mechanical Work from Folding-Based Protein Engines: From Single-Molecule Mechanochemical Cycles to Macroscopic Devices. *CCS Chem.* **2019**, *1*, 138–147.
15. Zheng, J.; Xiao, P.; Le, X.; Lu, W.; Théato, P.; Ma, C.; Du, B.; Zhang, J.; Huang, Y.; Chen, T. Mimosa Inspired Bilayer Hydrogel Actuator Functioning in Multi-Environments. *J. Mater. Chem. C* **2018**, *6*, 1320–1327.
16. Zhao, Q.; Yang, X.; Ma, C.; Chen, D.; Bai, H.; Li, T.; Yang, W.; Xie, T. A Bioinspired Reversible Snapping Hydrogel Assembly. *Mater. Horiz.* **2016**, *3*, 422–428.
17. Sun, Z.; Yamauchi, Y.; Araoka, F.; Kim, Y. S.; Bergueiro, J.; Ishida, Y.; Ebina, Y.; Sasaki, T.; Hikima, T.; Aida, T. An Anisotropic Hydrogel Actuator Enabling Earthworm-Like Directed Peristaltic Crawling. *Angew. Chem. Int. Ed.* **2018**, *57*, 15772–15776.
18. Wei, S. X.; Lu, W.; Le, X. X.; Ma, C. X.; Lin, H.; Wu, B. Y.; Zhang, J. W.; Théato, P.; Chen, T. Bioinspired Synergistic Fluorescence-Color-Switchable Polymeric Hydrogel Actuators. *Angew. Chem. Int. Ed.* **2019**, *58*, 16243–16251.
19. Cheng, M. J.; Zhang, D. Q.; Zhang, S.; Wang, Z. K.; Shi, F. Tackling the Short-Lived Marangoni Motion Using a Supramolecular Strategy. *CCS Chem.* **2019**, *1*, 148–155.
20. Zhu, Q. L.; Du, C.; Dai, Y.; Daab, M.; Matejdes, M.; Breu, J.; Hong, W.; Zheng, Q.; Wu, Z. L. Light-Steered Locomotion of Muscle-Like Hydrogel by Self-Coordinated Shape Change and Friction Modulation. *Nat. Commun.* **2020**, *11*, 5166.

**DOI:** 10.31635/ccschem.022.202201942
**Citation:** *CCS Chem.* **2023**, 5, 704–717
**Link to VoR:** https://doi.org/10.31635/ccschem.022.202201942

21. He, X. M.; Sun, Y.; Wu, J. H.; Wang, Y.; Chen, F.; Fan, P.; Zhong, M. Q.; Xiao, S. W.; Zhang, D.; Yang, J. T.; Zheng, J. Dual-Stimulus Bilayer Hydrogel Actuators with Rapid, Reversible, Bidirectional Bending Behaviors. *J. Mater. Chem. C* **2019**, *7*, 4970–4980.
22. Fan, W. X.; Shan, C. Y.; Guo, H. Y.; Sang, J. W.; Wang, R.; Zheng, R. R.; Sui, K. Y.; Nie, Z. H. Dual-Gradient Enabled Ultrafast Biomimetic Snapping of Hydrogel Materials. *Sci. Adv.* **2019**, *5*, eaav7174.
23. Xiao, S. W.; Zhang, M. Z.; He, X. M.; Huang, L.; Zhang, Y. X.; Ren, B. P.; Zhong, M. Q.; Chang, Y.; Yang, J. T.; Zheng, J. Dual Salt- and Thermoresponsive Programmable Bilayer Hydrogel Actuators with Pseudo-Interpenetrating Double-Network Structures. *ACS Appl. Mater. Interfaces* **2018**, *10*, 21642–21653.
24. Tan, Y.; Wang, D.; Xu, H.; Yang, Y.; Wang, X. L.; Tian, F.; Xu, P.; An, W.; Zhao, X.; Xu, S. Rapid Recovery Hydrogel Actuators in Air with Bionic Large-Ranged Gradient Structure. *ACS Appl. Mater. Interfaces* **2018**, *10*, 40125–40131.
25. Hao, X. P.; Xu, Z.; Li, C. Y.; Hong, W.; Zheng, Q.; Wu, Z. L. Kirigami-Design-Enabled Hydrogel Multimorphs with Application as a Multistate Switch. *Adv. Mater.* **2020**, *32*, 2000781.
26. Thérien-Aubin, H.; Wu, Z. L.; Nie, Z. H.; Kumacheva, E. Multiple Shape Transformations of Composite Hydrogel Sheets. *J. Am. Chem. Soc.* **2013**, *135*, 4834–4839.
27. Zhang, F. L.; Zhou, J. J.; Gu, Z.; Yang, M.; Li, S. H.; Song, Y. Y.; Fan, J. B.; Meng, J. X.; Wu, P. Y.; Jiang, L.; Wang, S. T. Flexible Dry Hydrogel with Lamella-Like Structure Engineered via Dehydration in Poor Solvent. *CCS Chem.* **2019**, *1*, 533–543.
28. Jeon, I.; Cui, J.; Illeperuma, W. R. K.; Aizenberg, J.; Vlassak, J. J. Extremely Stretchable and Fast Self-healing Hydrogels. *Adv. Mater.* **2016**, *28*, 4678–4683.
29. Yan, B.; He, C. Y.; Chen, S.; Xiang, L.; Gong, L.; Gu, Y.C.; Zeng, H. B. Nanoconfining Cation- $\pi$ Interactions as a Modular Strategy to Construct Injectable Self-Healing Hydrogel. *CCS Chem.* **2021**, *3*, 2903–2916.
30. Deng, Y. K.; Yuan, Y.; Chen, Y. L. Covalently Cross-Linked and Mechanochemiluminescent Polyolefins Capable of Self-Healing and Self-Reporting. *CCS Chem.* **2020**, *2*, 1316–1324.
31. Li, S. H.; Li, Y. X.; Wang, Y. T.; Pan, H. Y.; Sun, J. Q. Highly Stretchable, Elastic, Healable, and Ultra-Durable Polyvinyl Alcohol-Based Ionic Conductors Capable of Safe Disposal. *CCS Chem.* **2021**, *3*, 3360–3370.
32. Wu, B. Y.; Jian, Y. K.; Le, X. X.; Lin, H.; Wei, S. X.; Lu, W.; Zhang, J. W.; Zhang, A. F.; Huang, C. F.; Chen, T. Supramolecular Fabrication of Complex 3D Hollow Polymeric Hydrogels with Shape and Function Diversity. *ACS Appl. Mater. Interfaces* **2019**, *11*, 48564–48573.
33. Ji, X. F.; Zhao, L.; Hu, Y. B.; Xie, H. L.; Wu, W. J.; Song, F. Y.; Liu, H. X.; Wang, J. G.; Jiang, M. J.; Lam, J. W. Y.; Tang, B. Z. Bioinspired Hydrogels with Muscle-Like Structure for AIE-gen-Guided Selective Self-Healing. *CCS Chem.* **2020**, *2*, 1146–1156.
34. Shah, D.; Yang, B.; Kriegman, S.; Levin, M.; Bongard, J.; Kramer-Bottiglio, R. Shape Changing Robots: Bioinspiration, Simulation, and Physical Realization. *Adv. Mater.* **2020**, *33*, 2002882.
35. Xue, L.; Xiong, X.; Krishnan, B. P.; Puza, F.; Wang, S.; Zheng, Y.; Cui, J. Light-Regulated Growth from Dynamic Swollen Substrates for Making Rough Surfaces. *Nat. Commun.* **2020**, *11*, 963.
36. Jiang, P.; Lin, P.; Yang, C.; Qin, H.; Wang, X.; Zhou, F. 3D Printing of Dual-Physical Cross-linking Hydrogel with Ultrahigh Strength and Toughness. *Chem. Mater.* **2020**, *32*, 9983–9995.
37. Matsuda, T.; Kawakami, R.; Namba, R.; Nakajima, T.; Gong, J. P. Mechanoresponsive Self-Growing Hydrogels Inspired by Muscle Training. *Science* **2019**, *363*, 504–508.
38. Yu, K.; Feng, Z.; Du, H.; Xin, A.; Lee, K. H.; Li, K.; Su, Y.; Wang, Q.; Fang, N. X.; Daraio, C. Photosynthesis-Assisted Remodeling of Three-Dimensional Printed Structures. *Proc. Natl. Acad. Sci.* **2021**, *118*, e2016524118.
39. Zarket, B. C.; Raghavan, S. R. Onion-Like Multilayered Polymer Capsules Synthesized by A Bioinspired Inside-Out Technique. *Nat. Commun.* **2017**, *8*, 193.
40. Kwak, S. Y.; Giraldo, J. P.; Lew, T. T. S.; Wong, M. H.; Liu, P.; Yang, Y. J.; Koman, V. B.; McGee, M. K.; Olsen, B. D.; Strano, M. S. Polymethacrylamide and Carbon Composites that Grow, Strengthen, and Self-Repair using Ambient Carbon Dioxide Fixation. *Adv. Mater.* **2018**, *30*, 1804037.
41. Ma, S. H.; Yan, C. Y.; Cai, M. R.; Yang, J.; Wang, X. L.; Zhou, F.; Liu, W. M. Continuous Surface Polymerization via Fe(II)-Mediated Redox Reaction for Thick Hydrogel Coatings on Versatile Substrates. *Adv. Mater.* **2018**, *30*, 1803371.
42. Yin, Z. H.; Song, G. B.; Jiao, Y.; Zheng, P.; Xu, J. F.; Zhang, X. Dissipative Supramolecular Polymerization Powered by Light. *CCS Chem.* **2019**, *1*, 335–342.
43. Qi, X. D.; Yang, L.; Hou, Y.; Zhu, J. Q.; Yang, M.; Feng, S. H. A Self-Strengthening Epidermis-Like Smart Coating Enabled by Dynamic Iron Sequestration. *CCS Chem.* **2020**, *2*, 2655–2668.
44. Ding, P.; Huang, J. N.; Wei, C.; Liu, W.; Zhou, W. J.; Wang, J. H.; Wang, M. W.; Guo, X. H.; Stuart, M. A. C.; Wang, J. Y. Efficient and Generic Preparation of Diverse Polyelectrolyte Nanogels by Electrostatic Assembly Directed Polymerization. *CCS Chem.* **2020**, *2*, 1016–1025.
45. Shi, J. Z.; Jia, H. Y.; Chen, H.; Wang, X.; Xu, J. F.; Ren, W. P.; Zhao, J.; Zhou, X.; Dong, Y. C.; Liu, D. S. Concentration Insensitive Supramolecular Polymerization Enabled by Kinetically Interlocking Multiple-Units Strategy. *CCS Chem.* **2019**, *1*, 296–303.
46. Xu, R. N.; Zhang, Y. L.; Ma, S. H.; Ma, Z. F.; Yu, B.; Cai, M. R.; Zhou, F. A Universal Strategy for Growing a Tenacious Hydrogel Coating from a Sticky Initiation Layer. *Adv. Mater.* **2022**, *34*, 2108889.
47. Zhu, J. J.; Chen, G. Y; Yu, L.; Xu, H. L.; Liu, X. K.; Sun, J. Q. Mechanically Strong and Highly Stiff Supramolecular Polymer Composites Repairable at Ambient Conditions. *CCS Chem.* **2020**, *2*, 280–292.
48. Wu, J.; Cai, L. H.; Weitz, D. A. Tough Self-healing Elastomers by Molecular Enforced Integration of Covalent and Reversible Networks. *Adv. Mater.* **2017**, *29*, 1702616.

**DOI:** 10.31635/ccschem.022.202201942
**Citation:** *CCS Chem.* **2023**, 5, 704–717
**Link to VoR:** https://doi.org/10.31635/ccschem.022.202201942